Fitting surfaces with the Miura tessellation

H. Nassar, Arthur Lebée, Laurent Monasse

Fitting surfaces with the Miura tessellation

H. Nassar, A. Lebée, L. Monasse

Abstract: *The paper characterizes Miura surfaces defined as smooth surfaces that the regular periodic Miura ori can fit in the limit where the size of the creases is infinitely small compared to the typical radius of curvature. Based on a model due to Schenk and Guest, the Miura crease pattern is enriched so as to allow access to non-planar configurations. In contrast with previous work where the pattern is modified in order to fit different target surfaces, here we are interested in the converse problem of determining all the surfaces that can be fitted by one and the same pattern. The central result is a constrained nonlinear partial differential equation satisfied by the parametrization of any Miura surface. As an application, examples of bounded and unbounded Miura surfaces are presented along with a complete classification of axisymmetric and ruled ones.*

1 Introduction

Finding the surfaces that the plane can deform into and fit under various kinematical constraints is a problem with a long history. Euler proved that an inextensible plane can only fit those surfaces qualified as developable such as cylinders and cones. Later, Gauss established a connection between curvature and in-plane deformations in the context of his "Theorema Egregium". Developable surfaces are thus characterized as surfaces with vanishing Gaussian curvature. Armed with Gauss' theorem, Chebyshev tackled the problem of clothing curved surfaces [Ghys 11]. He mathematically modeled a cloth as a plane grid of inextensible threads now known as a Chebyshev grid. As the cloth deforms, the grid can be bent and sheared but cannot be stretched or compressed. Recently, it was proven that Chebyshev grids can cover any surface with a sufficiently small total absolute Gaussian curvature [Samelson and Dayawansa 12, Masson and Monasse 16]. The relevance of these and other fitting problems to the mechanics of plates and shells hardly needs emphasis. We mention the application of Chebyshev grids to the design of gridshells useful in architecture [Douthe et al. 09, Baverel et al. 12].

Rigid folding constitutes another class of kinematical constraints. It is well-known among origamists that fold tessellations allow for inextensible paper to fit curved surfaces in a way that challenges Euler's result [Lebée 15]. Euler had precluded folding by requiring smoothness whereas in the case of origami, paper is allowed to fold along predefined crease lines. Motivated by similar considerations, Resch and Christiansen famously attempted to fold a periodic crease pattern into

an egg, namely the Vegreville Easter egg. The pattern was designed by Resch and is now referred to as the Ron Resch pattern [Resch and Christiansen 70]. After six months of computer-assisted trials, they failed [Blinn 88]. Their final design introduced cuts that transformed Resch's pattern into the so-called Kagome lattice capable of fitting surfaces admitting a conformal metric, i.e., surfaces that can be flattened by applying some isotropic, although inhomogeneous, in-plane strain field [Konaković et al. 16].

Lately, significant efforts, with remarkable outcomes, have been made to design crease patterns that can be folded to fit target surfaces [Tachi 09, Tachi 13, Zhou et al. 15, Dudte et al. 16]. Here, we are interested in the converse question, that is in determining the surfaces that can be fitted with one and the same periodic origami tessellation, namely the regular periodic Miura ori. More specifically, we will characterize Miura surfaces defined as smooth surfaces that the Miura ori can fit in the limit where the size of the creases is infinitely small compared to the typical radius of curvature. Building on previous work [Schenk and Guest 13, Wei et al. 13, Nassar et al. 17a, Nassar et al. 17b], our central result is a constrained nonlinear partial differential equation satisfied by the parametrization of any Miura surface. As an application, various Miura surfaces are constructed and fitted. In particular, a complete classification of axisymmetric and ruled Miura surfaces is derived. But first, a useful algorithm allowing to construct a Miura ori based on the giving of some of its vertices is presented.

2 Discrete modeling of the Miura ori

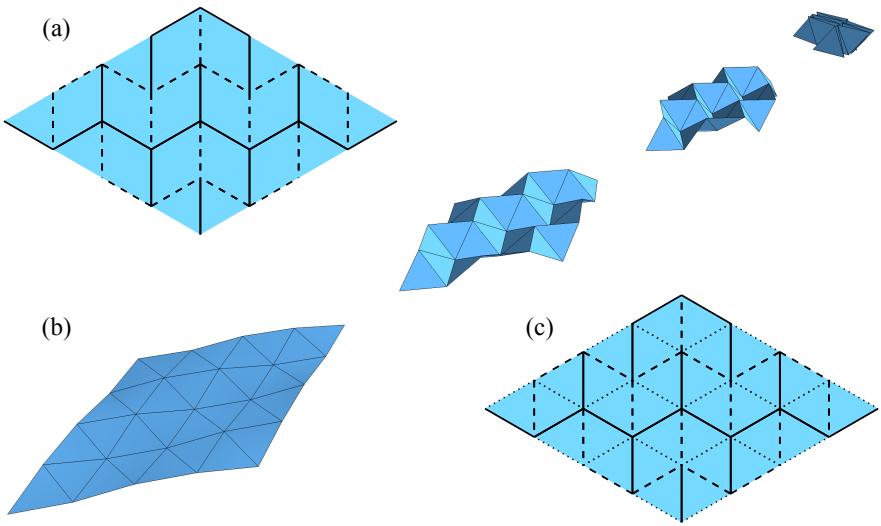

Figure 1: *The Miura crease pattern: (a) original pattern; (b) its unique deformation mode; (c) modified pattern.*

The Miura ori crease pattern is depicted on Figure 1a. The pattern can be folded along edges: solid and dashed lines represent valley and mountain folds respectively. If faces remain rigid then the only deformation mode of the Miura ori is the one represented on Figure 1b. Physical models, say made out of paper, of the Miura ori exhibit however other in-plane and out-of-plane modes that require the faces to bend. To explain these modes within the framework of rigid origami, a modified, enriched, crease pattern can be introduced [Schenk and Guest 13]. It includes additional creases, namely the dotted lines in Figure 1c, that can be folded either in mountains or in valleys. It is this modified pattern that is of interest here. We further restrict our attention to the regular Miura ori, the one whose all edges are equal in length, for simplicity.

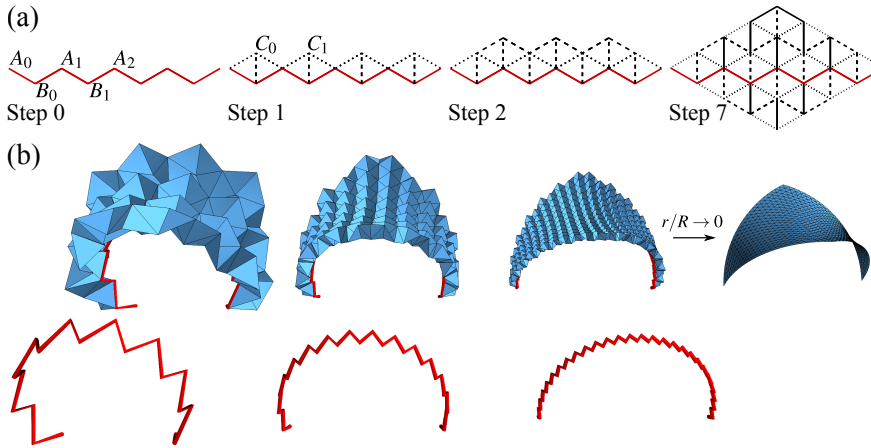

Figure 2: *(a) Algorithm: construction by zigzag propagation. (b) Convergence study: surfaces spanned by a uniform circular zigzag as the edge size decreases.*

All possible configurations of a Miura ori can be spanned by a fairly simple algorithm. First, assume given the three vertices A_0, B_0 and A_1 shown on Figure 2a and that the oriented angle (B_0A_1, B_0A_0) is in the interval $]0, 2\pi/3]$. Then, vertex C_0 belongs to the intersection of three spheres of equal radii and centered on A_0, B_0 and A_1. Although in general two intersection points exist, the position of C_0 must accommodate a mountain fold along B_0C_0. Thus, C_0 is the unique intersection of the described spheres that is located above the plane $(A_0B_0A_1)$. By iterating this procedure, if the red zigzag of Figure 2a is given at step 0, the next dotted zigzag can be uniquely determined in step 1. Then the construction is pursued until one zigzag exhibits an incompatible angle smaller than 0 or larger than $2\pi/3$, or until the current zigzag contains a single point. In this manner, the Miura ori can be uniquely constructed by propagating one zigzag up and down. The construction can be formalized as the autonomous discrete Cauchy problem

$$\text{zigzag}_{n+1} - \text{zigzag}_n = \text{function}(\text{zigzag}_n) \tag{1}$$

where zigzag_0 is the initial red zigzag and is given. The above algorithm will terminate in $2N-1$ steps at most when zigzag_0 contains $2N+1$ points. However, it is expected that the algorithm will terminate sooner due to the appearance of angles incompatible with the inextensibility constraints.

The Miura ori spanned by in-plane uniform zigzags correspond to the states encountered in the flat-folding motion of Figure 1b. For circular zigzags embedded in a short cylinder of radius R with a uniform inner angle of $\pi/3$, the spanned Miura ori are illustrated on Figure 2b for a decreasing edge size r. It is seen then that as r/R approaches zero while other parameters remain the same, the Miura ori approaches a smooth saddle surface. The purpose of the next section is to characterize such smooth surfaces referred to as Miura surfaces.

3 Differential geometry of Miura surfaces

Hereafter, we present a set of algebraic identities satisfied by the metric and curvature of a general Miura surface. Each identity can be seen as the giving of either the in-plane or the out-of-plane Poisson's ratio of the Miura tessellation in specific directions [Schenk and Guest 13, Wei et al. 13]. Combined with relevant tools of differential geometry, the identities yield a nonlinear partial differential equation governing the parametrization of a general Miura surface. This equation constitutes the continuous equivalent to algorithm (1) and is the main result of the present paper. Last, given the parametrization of a Miura surface, we describe how the underlying fitting tessellation can be generated.

3.1 Parametrization and metric

Let $\mathscr{S}$ be a smooth surface and R be its minimum radius of curvature. We call $\mathscr{S}$ a Miura surface if the Miura ori with edge size r can fit it in the limit $r/R \to 0$. Let $\phi : (x,y) \in \mathbb{R}^2 \mapsto \mathscr{S} \subset \mathbb{R}^3$ be a parametrization of $\mathscr{S}$ where x and y are the curvilinear coordinates along vectors w and w^* respectively as shown on Figure 3. In other words, we set

$$\phi_x = w/r, \quad \phi_y = w^*/r, \tag{2}$$

with $\square_x \equiv \partial_x \square$ and $\square_y \equiv \partial_y \square$. The first fundamental form of $\mathscr{S}$, also known as the metric, in the parametrization ϕ then reads

$$I = \begin{bmatrix} \langle \phi_x, \phi_x \rangle & \langle \phi_x, \phi_y \rangle \\ \langle \phi_x, \phi_y \rangle & \langle \phi_y, \phi_y \rangle \end{bmatrix} = \begin{bmatrix} 4\sin^2(\theta/2) & 0 \\ 0 & 4\cos^2(\theta^*/2) \end{bmatrix} \equiv \begin{bmatrix} 4s^2 & 0 \\ 0 & 4c^{*2} \end{bmatrix}. \tag{3}$$

Therein, we introduced the angles θ and θ^* of Figure 3 and used the fact that w is orthogonal to w^* due to mirror symmetry. For later purposes, similarly define $c \equiv \cos(\theta/2)$ and $s^* \equiv \sin(\theta^*/2)$. It is then elementary, although not straightforward [Schenk and Guest 13, Wei et al. 13, Nassar et al. 17a], to check that

$$2cc^* = 1. \tag{4}$$

Angles $\theta \equiv \theta(x,y)$ and $\theta^* \equiv \theta^*(x,y)$ determine the folding state of the Miura

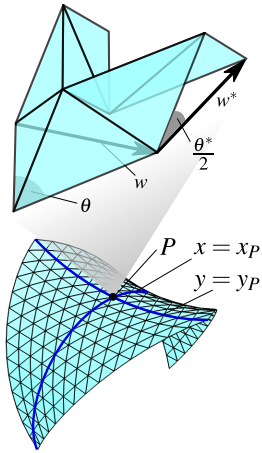

Figure 3: *A Miura surface: a blow-up of a neighborhood centered on a point P reveals the microstructure of the Miura ori. The underlying vectors w and w* are tangent to the surface and define the coordinate system* (x,y).

ori in the vicinity of a point $P(x,y)$ of the fitted surface $\mathscr{S}$: for $(\theta = 0, \theta^* = 2\pi/3)$, the Miura ori is fully folded whereas for $(\theta = 2\pi/3, \theta^* = 0)$, it is fully unfolded. In any case, (θ, θ^*) remains in the rectangle $[0, 2\pi/3]^2$. However, we shall assume $(\theta, \theta^*) \in]0, 2\pi/3] \times [0, 2\pi/3[$ so as to keep I from being singular.

3.2 Second fundamental form

Let $\hat{n} = \phi_x \times \phi_y / (4sc^*)$ be the unit vector directly normal to $\mathscr{S}$. The second fundamental form is defined as

$$II = \begin{bmatrix} \langle \phi_{xx}, \hat{n} \rangle & \langle \phi_{xy}, \hat{n} \rangle \\ \langle \phi_{xy}, \hat{n} \rangle & \langle \phi_{yy}, \hat{n} \rangle \end{bmatrix} \equiv \begin{bmatrix} e & f \\ f & g \end{bmatrix}. \tag{5}$$

Together, forms I and II allow to determine the various curvatures of $\mathscr{S}$. For instance, the normal curvatures in the directions x and y are respectively given by

$$\kappa^x = \frac{e}{\|\phi_x\|^2} = \frac{e}{4s^2}, \quad \kappa^y = \frac{g}{\|\phi_y\|^2} = \frac{g}{4c^{*2}}, \tag{6}$$

whereas the Gaussian and mean curvatures are

$$K = \frac{eg - f^2}{16 s^2 c^{*2}}, \quad H = \frac{ec^{*2} + gs^2}{8 s^2 c^{*2}}. \tag{7}$$

Remarkably, it was proven that the normal curvatures of the Miura ori satisfied the identity

$$\frac{\kappa^y}{\kappa^x} = -\tan^2(\theta/2) = -\frac{s^2}{c^2} \quad \text{or} \quad ec^{*2} + gc^2 = 0, \tag{8}$$

in the context of infinitesimal strains, i.e., $\theta(x,y) = \theta_0 + \delta\theta(x,y), \delta\theta \ll \theta_0$ [Schenk and Guest 13, Wei et al. 13]. Fortunately, using two-scale asymptotic expansions, it is possible to demonstrate that the above identity holds for finite strains as well but

only in the homogenization limit $r/R \ll 1$ [Nassar et al. 17a]. The interested reader is referred to the cited papers for proofs.

As an important corollary, note that e and g have opposite signs so that K is necessarily negative: all Miura surfaces are saddle-shaped.

3.3 The fitting problem

Based on the above results, we now derive a continualized version of algorithm (1), i.e., its asymptotic equivalent written in differential form. For that purpose, we express the vectors ϕ_{xx}, ϕ_{xy} and ϕ_{yy} in the basis $(\phi_x, \phi_y, \hat{n})$. This amounts to calculating the Christoffel symbols [Ciarlet 06]. We find

$$\begin{aligned}
\phi_{xx} &= \frac{(s^2)_x}{2s^2}\phi_x - \frac{(s^2)_y}{2c^{*2}}\phi_y + e\hat{n},\\
\phi_{xy} &= \frac{(s^2)_y}{2s^2}\phi_x + \frac{(c^{*2})_x}{2c^{*2}}\phi_y + f\hat{n},\\
\phi_{yy} &= -\frac{(c^{*2})_x}{2s^2}\phi_x + \frac{(c^{*2})_y}{2c^{*2}}\phi_y + g\hat{n}.
\end{aligned} \tag{9}$$

Then, thanks to equations (4) and (8), it is straightforward to check that the parametrization of a Miura surface satisfies the constrained nonlinear partial differential equation

$$\frac{\phi_{xx}}{1-\langle\phi_x,\phi_x\rangle/4} + \frac{\phi_{yy}}{\langle\phi_y,\phi_y\rangle/4} = 0, \tag{10a}$$

$$(1-\langle\phi_x,\phi_x\rangle/4)\langle\phi_y,\phi_y\rangle = 1, \tag{10b}$$

$$\langle\phi_x,\phi_y\rangle = 0, \tag{10c}$$

$$(\langle\phi_x,\phi_x\rangle, \langle\phi_y,\phi_y\rangle) \in]0,3]\times]1,4]. \tag{10d}$$

Equation (10) constitutes the fitting problem and summarizes our central result: if $\mathscr{S}$ is a Miura surface then it admits a parametrization solution to (10). Equation (10) is the asymptotic equivalent to equation (1) in the sense that, provided with an initial condition $(\phi(x,y=0), \phi_y(x,y=0))$, it generates a unique solution ϕ.

Having found a solution ϕ to (10), or equivalently to (3), (4) and (8), a fitting Miura ori with an arbitrarily small error can be constructed using algorithm (1). To do so,

- choose a small but finite discretization step r;
- construct the zigzag whose nodes are the A_n and B_m, $n = 0\ldots N$, $m = 0\ldots N-1$, where N is a large integer of the order of $1/r$; see Figure 2. Set[1] $A_n = \phi(x = nr, y = 0)$ and determine B_n such that $A_nB_n = B_nA_{n+1} = r$ and that the vector sum $B_nA_n + B_nA_{n+1}$ is parallel to, say, $\phi_y(x = nr + r/2, y = 0)$;
- finally, feed the zigzag $(A_0B_0\ldots B_{N-1}A_N)$ into algorithm (1).

[1] Then, $A_{n+1} - A_n = r\phi_x + o(r)$ in accordance with equation (2).

3.4 Discussion

Various open questions revolving around the fitting problem are worthy of investigation. These exceed the scope of the present paper and we content ourselves with a number of comments concluding this section.

First, it is remarkable that the quantities figuring in (10b) and (10c) are conserved in some sense. As a matter of fact, assuming only (10a) holds *a priori*, projecting onto ϕ_x and ϕ_y respectively yields

$$\begin{aligned}\frac{\partial_x \langle \phi_x, \phi_y \rangle}{1 - \langle \phi_x, \phi_x \rangle / 4} &= -\frac{1}{2} \partial_y \ln[(1 - \langle \phi_x, \phi_x \rangle / 4) \langle \phi_y, \phi_y \rangle], \\ \frac{\partial_y \langle \phi_x, \phi_y \rangle}{1 - \langle \phi_x, \phi_x \rangle / 4} &= \frac{1}{2} \partial_x \ln[(1 - \langle \phi_x, \phi_x \rangle / 4) \langle \phi_y, \phi_y \rangle].\end{aligned} \tag{11}$$

Now add the assumption that ϕ satisfies the constraints (10b) and (10c) at $y = 0$ and for all x. Then, the above equations can be understood as an autonomous Cauchy problem in the variable y and the unknown functions $\langle \phi_x, \phi_y \rangle$ and $\ln[(1 - \langle \phi_x, \phi_x \rangle / 4) \langle \phi_y, \phi_y \rangle]$ with a vanishing initial condition. Therefore, by Cauchy-Lipschitz theorem, $\langle \phi_x, \phi_y \rangle$ and $\ln[(1 - \langle \phi_x, \phi_x \rangle / 4) \langle \phi_y, \phi_y \rangle]$ are identically null. That is: ϕ satisfies (10b) and (10c) for all x and y.

Therefore, due to this conservation result, it seems that formulating (10) as a Cauchy problem is advantageous. Indeed, by appending an initial condition compatible with (10b) and (10c), one would no longer need to worry about these constraints. Alternatively, problem (10) can be formulated as a Dirichlet problem. In that case however, it is not clear what boundary data will be compatible with (10b) and (10c).

Unfortunately, equation (10a) is elliptic and thus will generally lead to an ill-posed Cauchy problem [Alessandrini et al. 09]. That is, a general solution ϕ will be very sensitive to uncertainties and errors in the initial condition. In practice, when loop (1) is iterated long enough, a numerical instability appears. Then, the construction algorithm terminates prematurely before generating the full Miura tessellation. See Figures 9 and 10 below for examples.

In any case, finding what combinations of boundary/initial conditions guarantee existence, uniqueness and stability remains an open question of fundamental importance both practical and theoretical.

4 Case studies

In the following, we prove the existence of certain fittings based on the equations derived in the previous section. Specifically, we classify all axisymmetric Miura surfaces and we prove that all ruled surfaces can be realized as nearly flat-folded Miura surfaces with an arbitrarily small fitting error. The presented examples do not exhaust all possible Miura surfaces but illustrate the advantages that the continuum approach (10) brings over the discrete formulation (1).

4.1 Developable surfaces

Let $\mathscr{S}$ be a developable Miura surface, i.e., a surface with constantly vanishing Gaussian curvature $K = 0$. But since eg is already negative, equation (7) implies $e = g = f = 0$ so that $\mathscr{S}$ is a plane: the plane is the unique developable Miura surface.

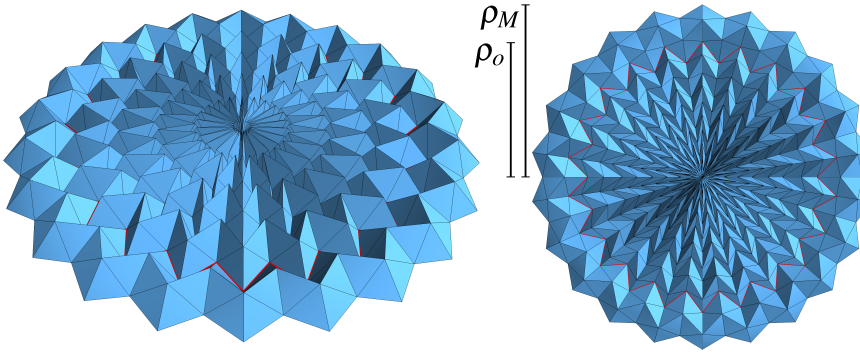

Figure 4: *Two views of the Miura rose.*

The plane can be fitted in a uniform manner, i.e., with constant θ, as shown on Figure 1b. Other non-uniform fittings of the plane, or at least parts thereof, can be generated at will by initiating algorithm (1) with an arbitrary in-plane zigzag. The Miura rose of Figure 4 is one such example where the initial zigzag is plane circular with a uniform inner angle $\theta_o = \pi/3$ and an arbitrary radius ρ_o. Here in particular, ρ_o was chosen so as to fit an integer number of unit cells in the circumference, e.g., $\rho_o = r\sin(\theta_o/2)/\sin(\pi/N)$ with N a large integer. It is then easy to see, as if by conservation of the number of unit cells, that ρ/s is uniform. Since $\sqrt{3}/2$ is the maximum value of s, the radius of the rose is given by $\rho_M = \frac{\sqrt{3}}{2\sin(\theta_o/2)}\rho_o$ and can be made arbitrarily large by making either ρ_o larger or θ_o smaller, both consistent with the fact that origami kinematics are scale-invariant.

The Miura rose is an example of an asymptotically axisymmetric plane fitting. Axisymmetry is hardly surprising the initial zigzag being axisymmetric itself. There exists however one other axisymmetric plane fitting generated by a non-axisymmetric initial zigzag. We call it the Miura ring and it is depicted on Figure 5a. The initial zigzag is visible on Figure 5b: it is fully collapsed on the inner circumference and fully extended on the outer one. Thus the radii ratio is $\rho_\mathrm{M}/\rho_\mathrm{m} = \max c^*/\min c^* = 2$.

Two remarks are in order here. First, the Miura ring cannot be fully constructed with a single initial zigzag. Indeed, by referring to Figure 2a, one sees that the initial zigzag only permits to construct a single "petal" shown on Figure 5a. The ring can then be spanned by successive rotations. Note that these rotations are compatible with the fitting of a single petal as is visible on the magnified view of Figure 5b. Second, the profile of the inner angle of the initial zigzag $\theta(x) = 2\arctan(2x/\rho_m)$ would have been tedious to extract from a discrete description of the Miura ori.

Here, it is obtained by solving equations (3) and (4) for a parametrization of the form $\phi(x,y) = (\rho(x)\cos(\alpha y), \rho(x)\sin(\alpha y), 0)$. It is in such circumstances that the usefulness of a continuous description of the Miura ori is undisputed.

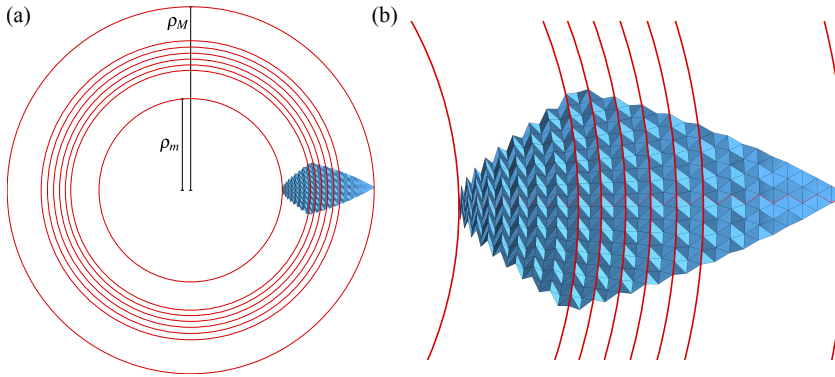

Figure 5: *The Miura ring: (a) rows of unit cells ($x = cste$) are concentric circles; (b) a magnified view. Note that $\rho_M/\rho_m \to 2$ as $r/\rho_m \to 0$.*

4.2 Axisymmetric surfaces of the first kind

A Miura surface is called axisymmetric about a z-axis if its fitting is asymptotically invariant by reflection along any plane containing the z-axis. Now, the Miura pattern has no more than two reflection[2] symmetries about the x and y axes. Therefore, axisymmetric Miura surfaces have their contours $\{x = x_o\}$ and $\{y = y_o\}$ contained in planes either parallel or orthogonal to the z-axis. Hence, axisymmetric Miura surfaces come in two flavors: surfaces with $\{y = y_o\} \subset \{z = z_o\}$ are said to be of the first kind; surfaces with $\{x = x_o\} \subset \{z = z_o\}$ are of the second kind.

Axisymmetric Miura surfaces are in particular invariant by rotation about the z-axis. Thus, surfaces of the first kind admit a parametrization of the form

$$\phi(x,y) = (\rho(y)\cos(\alpha x), \rho(y)\sin(\alpha x), z(y)). \tag{12}$$

By substitution into equations (3), (4) and (8), it is deduced that

$$\frac{\rho}{s} = \frac{\rho_o}{s_o}, \quad \rho'' = \frac{4\alpha^2\rho}{(\alpha^2\rho^2 - 4)^2}. \tag{13}$$

The second equation can be integrated once into

$$z' = \frac{\cos\beta}{c} = \frac{\cos\beta_o}{c_o}; \quad \sin\beta = \frac{\rho'}{2c^*}, \tag{14}$$

where β is the angle that the tangent plane makes with the z-axis. Therein, parameters $(\rho_o, \rho'_o, \theta_o)$ are determined by an initial condition, i.e., the initial zigzag.

[2]More precisely, one reflection and one glide reflection with a vanishingly small translation.

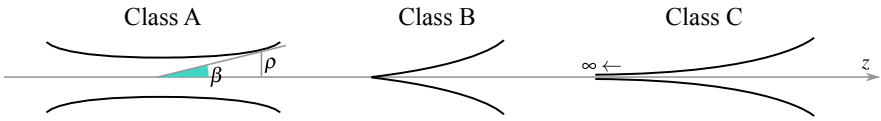

Figure 6: *Classification of axisymmetric Miura surfaces of the first kind.*

It can be argued that a Miura surface of the first kind belongs to one of the classes A, B and C schematically depicted on Figure 6. As a matter of fact,

- since $K < 0$, ρ is a convex function of z;
- ρ is bounded since s is;
- ρ cannot admit a horizontal asymptote other than 0 since $\rho \to \rho_\infty$ as $z \to \pm\infty$ implies $\kappa_y \to 0$ and, by identity (8), $s \to 0$ and $\rho \to 0$;
- and, if the range of existence of ϕ cannot be extended beyond a finite value of y denoted y_f, then $\theta(y = y_f)$ is equal to either 0 or $2\pi/3$.

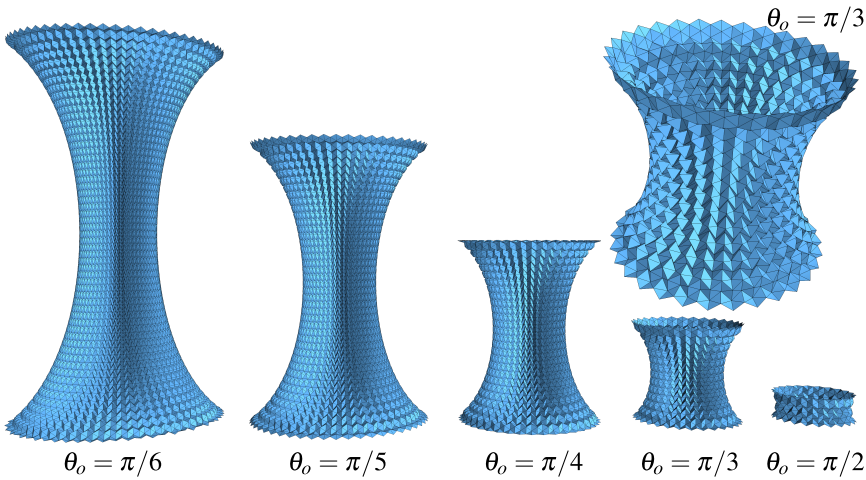

Figure 7: *Axisymmetric Miura surfaces of the first kind, class A: instances for varying θ_o and a vanishing β_o.*

Therefore,

- ρ can decrease from a maximum value ρ_M to reach a non-zero minimum ρ_m and then increase back to ρ_M; these profiles correspond to class A. In this case, at $\rho = \rho_m$, $\beta = 0$ and $\theta = \theta_m \neq 0$ so that

$$\frac{\cos\beta}{c} = \frac{1}{c_m} > 1. \tag{15}$$

- ρ can increase from a null *minimum* value $\rho_m = 0$ to reach a maximum value ρ_M; these profiles correspond to class B. Note that $\rho_m' \neq 0$ since otherwise ρ would be

uniformly null by Cauchy-Lipschitz theorem. Thus, $\theta_m = 0$ and $\beta_m \neq 0$ so that

$$\frac{\cos\beta}{c} = \cos\beta_m < 1. \tag{16}$$

- ρ can increase from a null *infimum non-minimum* value $\rho_m = 0$ to reach a maximum value ρ_M; such profiles correspond to class C. Here, as $\rho \to 0$, $\theta \to 0$ and $\beta \to 0$ so that

$$\frac{\cos\beta}{c} = 1. \tag{17}$$

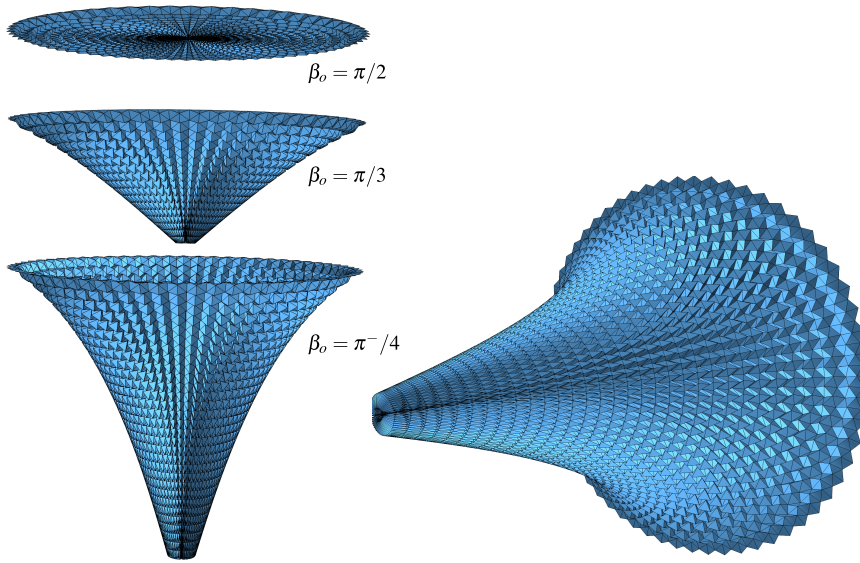

Figure 8: *Axisymmetric Miura surfaces of the first kind, class B: instances for varying β_o and a constant $\theta_o = \pi/2$.*

In summary, homotheties and rigid body motions aside, axisymmetric Miura surfaces of the first kind form a two-parameter family of surfaces parametrized by two angles, namely β_o and θ_o, and classified into three classes A, B and C depending on whether $\cos\beta_o/c_o$ is smaller, larger or equal to unity, respectively. Instances of class A are depicted on Figure 7 for a varying $\theta_o > 0$ and a vanishing β_o. Instances of class B are depicted on Figure 8 for a varying $\beta_o < \pi/4$ and a constant $\theta_o = \pi/2$. The unique surface of class C admits the implicit equation

$$z = \sqrt{\frac{4}{3}\rho_M^2 - \rho^2} - \frac{2}{\sqrt{3}}\rho_M \ln\left(\frac{\sqrt{4\rho_M^2 - 3\rho^2} + 2\rho_M}{\rho}\right). \tag{18}$$

We call it the Miura horn and it is depicted on Figure 9.

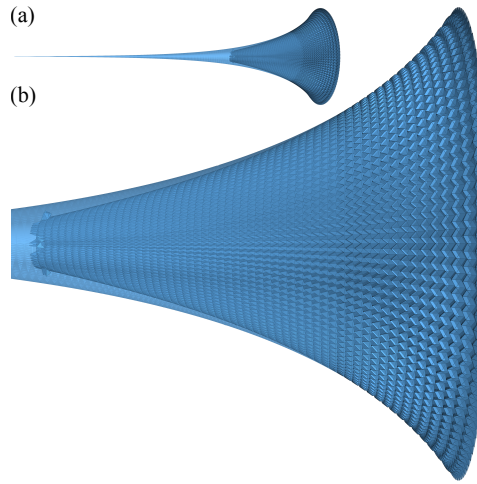

Figure 9: *The Miura horn or the unique axisymmetric Miura surface of the first kind, class C: (a) global view; (b) magnified view. Both the surface (semi-transparent, blue) and its discrete fitting (black edges) are depicted. The fitting reaches deeper into the tail with smaller errors as r decreases further but in any case fails to account for the infinite extension of the surface due to a visible numerical instability.*

Note that while constructing the fitting of the Miura horn, we have encountered a numerical instability that forbids the Miura tessellation from reaching deep into the tail of the horn; see Figure 9b. This constitutes a first example of the stability issues discussed in subsection 3.4 in connection with elliptic Cauchy problems. We will comment on another example hereafter.

4.3 Axisymmetric surfaces of the second kind

Axisymmetric Miura surfaces of the second kind admit a parametrization of the form

$$\phi(x,y) = (\rho(x)\cos(\alpha y), \rho(x)\sin(\alpha y), z(x)). \tag{19}$$

By substitution into equations (3), (4) and (8), two conserved quantities emerge:

$$\frac{\rho}{c^*} = \frac{\rho_o}{c_o^*}, \quad z'/2 = s\cos\beta = s_o\cos\beta_o. \tag{20}$$

Using similar techniques as before, these surfaces can be classified into two classes A and B. Surfaces of class A have a minimum non-vanishing angle $\theta = \theta_m$ attained at $\beta = 0$ and therefore constitute a one-parameter family of surfaces parametrized with $\theta_m \in]0, 2\pi/3[$. The unique surface of class B has a vanishing infimum $\theta_m = 0$ and is identical to the Miura ring. Here too, algorithm (1) cannot generate the full surface out of a single initial zigzag. Instead a portion can be constructed and then the surface spanned by successive rotations as described for the Miura ring of Figure 5. Surfaces and partial fittings are visible on Figure 10.

To construct the underlying tessellations, equation (20) needs to be integrated so as to determine the initial zigzag. Here, closed-form expressions are available and read

$$\rho = \sqrt{4c_o^2x^2 + 1}, \quad z = 2s_o x, \quad x \in [-s_o^*, s_o^*] \tag{21}$$

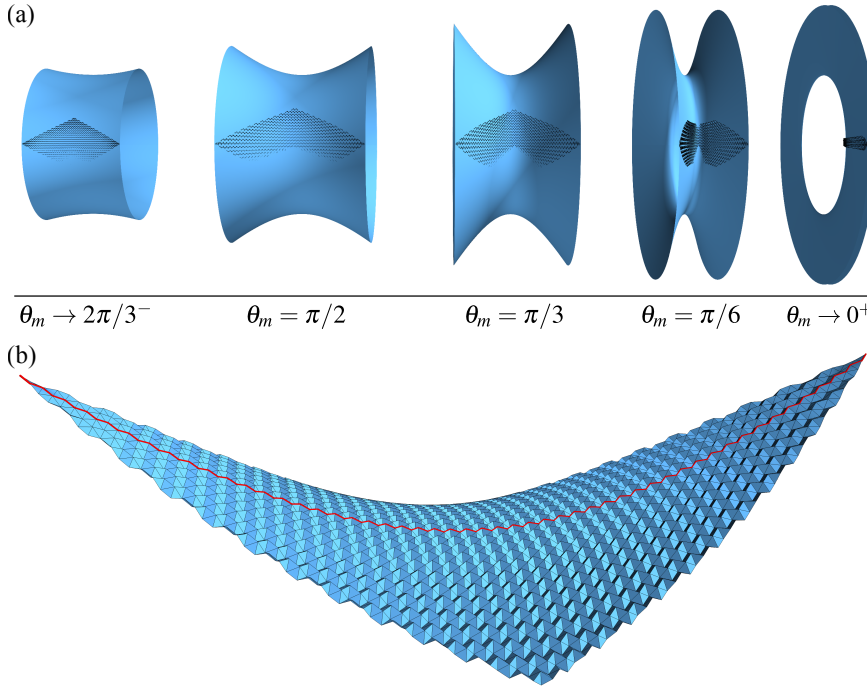

Figure 10: *Axisymmetric Miura surfaces of the second kind, class A: (a) instances for varying θ_m; (b) magnified view of the tessellation for $\theta_m = \pi/3$. The Miura ring, the unique surface of class B, is realized in the limit $\theta_m \to 0^+$.*

once the normalized initial conditions $(\theta_o = \theta_m, \rho_o = 1, \rho_o' = 0, z_o = 0)$ have been adopted. Last, as θ_m approaches 0, the numerical instability encountered with the Miura horn manifests here as well. By comparing the plots of Figure 10a, it is seen that for $\theta_m \leq \pi/6$, the construction of the tessellation terminates abruptly before reaching the rhomboidal shape characteristic of algorithm (1) (see Figure 2a).

4.4 Ruled surfaces

Call N and M the number of unit cells in the directions x and y respectively. So far, numbers N and M increased proportionally to R/r in such a manner that the constructed Miura surfaces maintained finite extents in the directions x and y of the order of Nr and Mr respectively. In this subsection, we explore Miura surfaces in the limit where θ uniformly approaches 0, that is in the regime $0 < \Theta \equiv \max(\theta) \ll 2\pi/3$. Accordingly, we let N grow at a faster rate inversely proportional to $r\Theta/R$ so that, as θ approaches 0 and the Miura ori flat-folds, a finite extent in the x direction is maintained.

It is then appropriate to rescale variable x by carrying the change of variables

$(X,Y) = (\Theta x, y)$. The fitting problem (10) becomes

$$\begin{aligned} \frac{\Theta^2 \phi_{XX}}{1-\Theta^2 \langle \phi_x, \phi_x \rangle/4} + \frac{\phi_{YY}}{\langle \phi_Y, \phi_Y \rangle/4} &= 0, \\ (1-\Theta^2 \langle \phi_X, \phi_x \rangle/4) \langle \phi_Y, \phi_Y \rangle &= 1, \\ \langle \phi_X, \phi_Y \rangle &= 0, \\ (\Theta^2 \langle \phi_X, \phi_X \rangle, \langle \phi_Y, \phi_Y \rangle) &\in]0,3] \times]1,4]. \end{aligned} \tag{22}$$

Passing to the limit then yields

$$\phi_{YY} = 0, \quad \langle \phi_Y, \phi_Y \rangle = 1, \quad \langle \phi_X, \phi_Y \rangle = 0. \tag{23}$$

Finally, integrating twice, the parametrization of a Miura surface in the flat-folding limit turns out to admit the expression

$$\phi(X,Y) = Yu(X) + v(X), \tag{24}$$

with u unitary and orthogonal to v. These parametrizations cover all ruled surfaces. We therefore conclude that the set of nearly flat-folded Miura surfaces is exactly the set of all ruled surfaces.

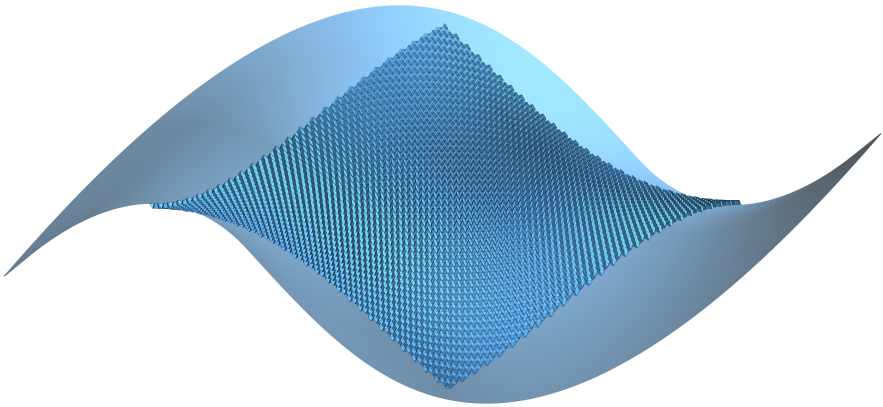

Figure 11: *Fitting a helicoid: The edges of the Miura ori are rendered in black whereas the helicoid is rendered as a solid opaque surface. The fact that the edges are visible from both sides of the helicoid reflects the fact that the absolute fitting error is of the order of r.*

As a first example, recall that developable surfaces are ruled surfaces: they all can be fitted by a nearly-flat folded Miura ori. It is worth mentioning that our earlier result stating that the plane is the unique developable Miura surface holds as long as flat-folding is precluded as a singularity. In the present flat-folding limit however,

all developable surfaces become Miura surfaces. We have already encountered two nearly developable Miura surfaces while classifying the axisymmetric surfaces of the first kind. Indeed, looking at Figures 7 and 8, it is easy to see that, as θ_o approaches 0, both cylindrical and conical Miura surfaces can be obtained.

The helicoid is a second example of a ruled but non-developable Miura surface. A helicoid with thread L is spanned in the limit $(\theta_o \to 0, r/L \to 0)$ by a rectilinear zigzag with a uniform inner angle θ_o and with teeth rotating around its axis with a uniform step of $2\pi/N$ such that $2\sin(\theta_o/2)Nr = L$. The result is shown on Figure 11. The parameters used are such that $r/L \sim 1/100$ and θ_o as large[3] as $\pi/3$.

5 Conclusion

A continuous characterization of the deformation modes of an enriched Miura ori, or equivalently, of the smooth surfaces that it can fit, has proven advantageous on many levels. It permitted to predict the existence of various Miura surfaces and in particular to establish a complete classification of axisymmetric and ruled ones. It also allowed to gain deeper insight into the discrete kinematics of the tessellation and to raise a number of issues regarding its stability in connection to the type of enforced boundary/initial conditions for instance. Not to mention that the present purely kinematical study is a first step in establishing a continuum mechanical model of the tessellation that takes into account elasticity effects.

References

[Alessandrini et al. 09] G. Alessandrini, L. Rondi, E. Rosset, and S. Vessella. "The stability for the Cauchy problem for elliptic equations." *Inverse Probl.* 25 (2009), 123004.

[Baverel et al. 12] O. Baverel, J. F. Caron, F. Tayeb, and L. Du Peloux. "Gridshells in composite materials: Construction of a 300 m^2 forum for the solidays' festival in Paris." *Struct. Eng. Int.* 22 (2012), 408–414.

[Blinn 88] J.F. Blinn. "The world's largest easter egg and what came out of it." *IEEE Comput. Graph. Appl.* 8 (1988), 16–23.

[Ciarlet 06] P. G. Ciarlet. *An introduction to differential geometry with applications to elasticity*. Dordrecht: Springer, 2006.

[Douthe et al. 09] C. Douthe, J. F. Caron, and O. Baverel. "Gridshell in composite materials: Towards large span shelters." *Eur. J. Environ. Civ. Eng.* 13 (2009), 1083–1093.

[Dudte et al. 16] L. H. Dudte, E. Vouga, T. Tachi, and L. Mahadevan. "Programming curvature using origami tessellations." *Nat. Mater.* 15 (2016), 583–588.

[Ghys 11] E. Ghys. "Sur la coupe des vêtements: Variation autour d'un thème de Tchebychev." *L'Enseignement Mathématique* 57 (2011), 165–208.

[3] Why asymptotics carried in the vicinity of 0 should be valid near $\pi/3$ is a mystery. An explanation might be found in the fact that (24) is identical to a first order Taylor expansion in Y. But this will not be pursued here.

[Konaković et al. 16] M. Konaković, K. Crane, B. Deng, S. Bouaziz, D. Piker, and M. Pauly. "Beyond developable: computational design and fabrication with auxetic materials." *ACM Trans. Graph.* 35 (2016), 89.

[Lebée 15] A. Lebée. "From folds to structures, a review." *Int. J. Sp. Struct.* 30 (2015), 55–74.

[Masson and Monasse 16] Y. Masson and L. Monasse. "Existence of global Chebyshev nets on surfaces of absolute Gaussian curvature less than 2π." *J. Geom.* 108 (2016), 25–32.

[Nassar et al. 17a] H. Nassar, A. Lebée, and L. Monasse. "Curvature, metric and parametrization of origami tessellations: theory and application to the eggbox pattern." *Proc. R. Soc. A* 473 (2017), 20160705.

[Nassar et al. 17b] H. Nassar, A. Lebée, and L. Monasse. "Macroscopic deformation modes of origami tessellations and periodic pin-jointed trusses: the case of the eggbox." In *Proc. IASS*. Hamburg, 2017.

[Resch and Christiansen 70] R. D. Resch and H. Christiansen. "The design and analysis of kinematic folded-plate systems." *Proc. IASS Symp. folded plates Prism. Struct.*

[Samelson and Dayawansa 12] S. L. Samelson and W. P. Dayawansa. "On the existence of global Tchebychev nets." *Trans. Am. Math. Soc.* 347 (2012), 651–660.

[Schenk and Guest 13] M. Schenk and S. D. Guest. "Geometry of Miura-folded metamaterials." *Proc. Natl. Acad. Sci.* 110 (2013), 3276–3281.

[Tachi 09] T. Tachi. "Generalization of rigid foldable quadrilateral mesh origami." In *Proc. IASS*, pp. 2287–2294. Valencia, 2009.

[Tachi 13] T. Tachi. "Designing freeform origami tessellations by generalizing Resch's patterns." *J. Mech. Des.* 135 (2013), 111006.

[Wei et al. 13] Z. Y. Wei, Z. V. Guo, L. Dudte, H. Y. Liang, and L. Mahadevan. "Geometric mechanics of periodic pleated origami." *Phys. Rev. Lett.* 110 (2013), 215501.

[Zhou et al. 15] X. Zhou, H. Wang, and Z. You. "Design of three-dimensional origami structures based on a vertex approach." *Proc. R. Soc. A* 471 (2015), 20150407.

Hussein Nassar
Department of Mechanical and Aerospace Engineering, University of Missouri, Columbia
e-mail: nassarh@missouri.edu

Arthur Lebée
Laboratoire Navier (UMR 8205), École des Ponts IFSTTAR, CNRS, Université Paris Est,
e-mail: arthur.lebee@enpc.fr

Laurent Monasse
Université Côte d'Azur, Inria, Team COFFEE, and Laboratoire J.A. Dieudonné (UMR 7351),
CNRS, Nice e-mail: laurent.monasse@inria.fr